Nuclear Science and Techniques (2025) 36:29
https://doi.org/10.1007/s41365-024-01609-9

Isospin splitting of the Dirac mass probed using the relativistic Brueckner–Hartree–Fock theory

Pianpian Qin[1] · Qiang Zhao[2] · Hui Tong[3] · Chencan Wang[4] · Sibo Wang[1]

Received: 2 July 2024 / Revised: 23 August 2024 / Accepted: 16 September 2024 / Published online: 11 January 2025

Abstract
The isospin splitting of the Dirac mass obtained using the relativistic Brueckner–Hartree–Fock (RBHF) theory was thoroughly investigated. From the perspective in the full Dirac space, the long-standing controversy between the momentum-independent approximation (MIA) method and the projection method on the isospin splitting of the Dirac mass in asymmetric nuclear matter was analyzed in detail. We found that the *assumption procedure* of the MIA method, which assumes that single-particle potentials are momentum independent, is not a sufficient condition that directly leads to the opposite sign of the isospin splitting of the Dirac mass, whereas the *extraction procedure* of the MIA method, which extracts single-particle potentials from single-particle potential energy, changes the sign. A formal expression of the Dirac mass was obtained by approximately solving a set of equations involved in the *extraction procedure*. The opposite isospin splitting of the Dirac mass was mainly caused by the *extraction procedure*, which forcibly assumed that the momentum dependence of the single-particle potential energy was in a quadratic form, in which the strength was solely determined by a constant scalar potential. Improved understanding of the isospin splitting of the Dirac mass from ab initio calculations could enhance our knowledge of neutron-rich systems, such as exotic nuclei and neutron stars.

Keywords Dirac mass · Relativistic Brueckner–Hartree–Fock theory · Single-particle potential · Momentum dependence

This work was supported in part by the China Postdoctoral Science Foundation under grant No. 2021M700610, the National Natural Science Foundation of China (NSFC) (No. 12205030), the Fundamental Research Funds for the Central Universities (No. 2024CDJXY022), and the Institute for Basic Science (No. IBS-R031-D1). Part of this study was achieved using the supercomputer OCTOPUS at the Cybermedia Center, Osaka University under the support of the Research Center for Nuclear Physics of Osaka University and the High Performance Computing Resources in the Research Solution Center, Institute for Basic Science.

✉ Sibo Wang
sbwang@cqu.edu.cn

1 Department of Physics and Chongqing Key Laboratory for Strongly Coupled Physics, Chongqing University, Chongqing 401331, China

2 Center for Exotic Nuclear Studies, Institute for Basic Science, Daejeon 34126, Korea

3 Helmholtz-Institut für Strahlen- und Kernphysik and Bethe Center for Theoretical Physics, Universität Bonn, Bonn D-53115, Germany

4 School of Physics and Astronomy, Sun Yat-Sen University, Zhuhai 519082, China

1 Introduction

To understand the properties of nuclear many-body systems that start from realistic nucleon–nucleon (*NN*) interactions is still challenging. The repulsive core of realistic *NN* interactions causes a strong correlation for the many-body wave function and requires advanced many-body methods that go beyond mean field [1–6]. The Brueckner–Hartree–Fock (BHF) theory [7] is one of the representative nuclear many-body methods, which is characteristic for its capacity to soften the realistic *NN* interaction to an effective *G* matrix in nuclear medium. The BHF theory can be derived as a two-hole-line truncation to the general Bethe–Brueckner–Goldstone expansion theory [1, 8], where the ground-state properties of the nuclear many-body systems are calculated order by order according to the number of independent hole lines contained in the expansion diagrams [8]. Since 1960s, it has been found that the saturation points of symmetric nuclear matter (SNM) calculated using the BHF theory with different two-body interactions are located on a Coester line [9], which deviates systematically from empirical values. To address this issue within the nonrelativistic framework is to introduce three-body forces [10–15].

In 1980, a major modification of the saturation properties of SNM was obtained by including a relativistic description of the nucleon motion [16]. Through this pioneering work, significant efforts have been made to develop the relativistic Brueckner–Hartree–Fock (RBHF) theory [17–20]. Starting from the Bonn potential [21], the saturation points of SNM obtained using the RBHF theory have been shifted remarkably close toward the empirical values, without introducing explicit three-body forces. The success of the RBHF theory has been understood by the fact that relativistic effects contribute a particular part of the three-body force [12, 14, 22] through virtual nucleon–antinucleon excitations in the intermediate states (known as Z diagrams) [23, 24].

An essential point of the RBHF theory is the use of the Dirac equation to describe the single-nucleon motion in the mean field, that is, the single-particle potential (SPP). An SPP operator is generally divided into scalar and vector components [25]. They can be obtained from an effective G matrix in a self-consistent manner. In principle, the calculations of SPPs and the G matrix should be performed in the full Dirac space, where both the positive-energy states (PESs) and negative-energy states (NESs) are included. However, owing to the complexities of these procedures, RBHF calculations are generally performed without NESs using approximate methods, such as the momentum-independent approximation (MIA) method [22, 26–30] and the projection method [20, 31–35], to perform the Hartree–Fock calculations.

The MIA method assumes that the SPPs are independent of the momentum and extracts the SPPs from single-particle potential energies calculated at two selected momenta. In the projection method, the elements of the G matrix are projected onto a complete set of Lorentz invariant amplitudes [19], from which the SPPs are calculated. Because the G matrix coupled to the NESs is not considered, the SPPs obtained using these two methods are ambiguous [31, 36, 37].

The Dirac mass M^*_{D}, a key quantity in relativistic nuclear physics, is defined using the scalar component of the nucleon self-energy within the Dirac equation. This quantity is crucial for describing medium effects in nuclear many-body systems, as highlighted in various studies [38–40]. An important aspect of the Dirac mass is its isospin splitting $M^*_{\mathrm{D,n}} - M^*_{\mathrm{D,p}}$, which directly reflects the isovector properties of *NN* interactions [41, 42]. It is essential to clarify that the Dirac mass should not be confused with the nonrelativistic effective mass, which characterizes the momentum and energy dependence of the Schrödinger equivalent potential [43, 44]. Theoretical predictions of the Dirac mass based on realistic *NN* interactions mainly rely on the RBHF theory. However, there is a controversy regarding the sign of this isospin splitting [33, 45]. As pointed in Ref. [46] in 1997, the MIA method leads to $M^*_{\mathrm{D,n}} - M^*_{\mathrm{D,p}} > 0$, whereas the projection method indicates an opposite sign $M^*_{\mathrm{D,n}} - M^*_{\mathrm{D,p}} < 0$. This discrepancy demonstrates significant differences in the isovector properties of asymmetric nuclear matter (ANM) when employing the MIA method versus the projection method in RBHF calculations.

Recently, self-consistent RBHF calculations in the full Dirac space have been achieved [37, 47, 48], which avoid the ambiguities suffered from the RBHF calculations without NESs. In ANM, the full solution predicts the sign $M^*_{\mathrm{D,n}} - M^*_{\mathrm{D,p}} < 0$ [48] and clarifies the long-standing controversy between the MIA and projection methods on the isospin splitting of the Dirac mass. The RBHF theory has also been applied in the full Dirac space to study the nonrelativistic effective mass in nuclear matter [49], the properties of ^{208}Pb using a liquid droplet model [50], the tensor-force effects on nuclear matter [51], and the neutron star properties [52–54]. In this work, we aimed to thoroughly study the isospin splitting of the Dirac mass obtained using the RBHF calculations, particularly for the performance of the MIA method, in the full Dirac space viewpoint.

2 Theoretical framework

In the RBHF theory, the single-particle motion of a nucleon inside an infinite nuclear matter is described by the following Dirac equation:

$$\left\{\boldsymbol{\alpha}\cdot\boldsymbol{p}+\beta\left[M+\mathcal{U}_\tau(\boldsymbol{p})\right]\right\}u_\tau(\boldsymbol{p},s)=E_{p,\tau}u_\tau(\boldsymbol{p},s). \tag{1}$$

where $\boldsymbol{\alpha}$ and β are the Dirac matrices, M is the nucleon mass, $\boldsymbol{p}$ and $E_{p,\tau}$ are the momentum and single-particle energy, respectively, s denotes the spin, and $\tau = n, p$ denotes neutron n and proton p. The symbol u_τ in Eq. (1) represents the positive-energy Dirac spinor, whereas the negative-energy Dirac spinor v_τ is obtained using $v_\tau = \gamma_5 u_\tau$. The SPP operator $\mathcal{U}_\tau(\boldsymbol{p})$ can be decomposed into the scalar potential $U_{\mathrm{S},\tau}(p)$, the timelike and spacelike components of the vector potential $U_{0,\tau}(p)$ and $U_{\mathrm{V},\tau}(p)$ [25], respectively.

$$\mathcal{U}_\tau(\boldsymbol{p})=U_{\mathrm{S},\tau}(p)+\gamma^0U_{0,\tau}(p)+\boldsymbol{\gamma}\cdot\hat{\boldsymbol{p}}U_{\mathrm{V},\tau}(p). \tag{2}$$

where $\hat{\boldsymbol{p}}=\boldsymbol{p}/|\boldsymbol{p}|=\boldsymbol{p}/p$ is the unit vector parallel to the momentum $\boldsymbol{p}$. By calculating the matrix elements of $\mathcal{U}_\tau(\boldsymbol{p})$ as expanded by the PESs and NESs, that is, $\Sigma^{++}_\tau(p)$, $\Sigma^{-+}_\tau(p)$, and $\Sigma^{--}_\tau(p)$, the momentum-dependent SPPs can be determined uniquely using the following equation [37, 52]:

$$U_{\mathrm{S},\tau}(p)=\frac{\Sigma^{++}_\tau(p)-\Sigma^{--}_\tau(p)}{2}, \tag{3a}$$

$$U_{0,\tau}(p) = \frac{E^*_{p,\tau}}{M^*_{p,\tau}} \frac{\Sigma^{++}_\tau(p) + \Sigma^{--}_\tau(p)}{2} - \frac{p^*_\tau}{M^*_{p,\tau}} \Sigma^{-+}_\tau(p), \tag{3b}$$

$$U_{V,\tau}(p) = -\frac{p^*_\tau}{M^*_{p,\tau}} \frac{\Sigma^{++}_\tau(p) + \Sigma^{--}_\tau(p)}{2} + \frac{E^*_{p,\tau}}{M^*_{p,\tau}} \Sigma^{-+}_\tau(p). \tag{3c}$$

where the plus and minus signs in the superscripts denote the PESs and NESs, respectively. The effective quantities in Eq. (3) are defined as follows: $\boldsymbol{p}^*_\tau = \boldsymbol{p} + \hat{\boldsymbol{p}} U_{V,\tau}(p)$, $M^*_{p,\tau} = M + U_{S,\tau}(p)$, and $E^*_{p,\tau} = E_{p,\tau} - U_{0,\tau}(p)$. The effective mass $M^*_{p,\tau}$ is also known as the Dirac mass $M^*_{D,\tau}$.

The quantities $\Sigma^{++}_\tau(p)$, $\Sigma^{-+}_\tau(p)$, and $\Sigma^{--}_\tau(p)$ in Eq. (3) are calculated by summing up the effective G matrix elements with all the nucleons inside the Fermi sea.

$$\Sigma^{++}_\tau(p) = \sum_{s'\tau'} \int_0^{k_F^{\tau'}} \frac{d^3p'}{(2\pi)^3} \frac{M^*_{p',\tau'}}{E^*_{p',\tau'}} \langle \bar{u}_\tau(\boldsymbol{p}, 1/2) \bar{u}_{\tau'}(\boldsymbol{p}', s') \\ |\bar{G}^{++++}(W)| u_\tau(\boldsymbol{p}, 1/2) u_{\tau'}(\boldsymbol{p}', s')\rangle, \tag{4a}$$

$$\Sigma^{-+}_\tau(p) = \sum_{s'\tau'} \int_0^{k_F^{\tau'}} \frac{d^3p'}{(2\pi)^3} \frac{M^*_{p',\tau'}}{E^*_{p',\tau'}} \langle \bar{v}_\tau(\boldsymbol{p}, 1/2) \bar{u}_{\tau'}(\boldsymbol{p}', s') \\ |\bar{G}^{-+++}(W)| u_\tau(\boldsymbol{p}, 1/2) u_{\tau'}(\boldsymbol{p}', s')\rangle, \tag{4b}$$

$$\Sigma^{--}_\tau(p) = \sum_{s'\tau'} \int_0^{k_F^{\tau'}} \frac{d^3p'}{(2\pi)^3} \frac{M^*_{p',\tau'}}{E^*_{p',\tau'}} \langle \bar{v}_\tau(\boldsymbol{p}, 1/2) \bar{u}_{\tau'}(\boldsymbol{p}', s') \\ |\bar{G}^{-+-+}(W)| v_\tau(\boldsymbol{p}, 1/2) u_{\tau'}(\boldsymbol{p}', s')\rangle. \tag{4c}$$

where $\bar{G}$ is the antisymmetrized G matrix, k_F^τ is the Fermi momentum, and W denotes the starting energy. The additional factors M^*/E^* in Eq. (4) are attributed to the normalization of the Dirac spinors, that is, $\bar{u}u = 1, \bar{v}v = -1$. The effective interaction G matrix is the solution of the in-medium Thompson equation [26], which describes the two-body scattering.

$$G_{\tau\tau'}(\boldsymbol{q}', \boldsymbol{q}|\boldsymbol{P}, W) = V_{\tau\tau'}(\boldsymbol{q}', \boldsymbol{q}|\boldsymbol{P}) \\ + \int \frac{d^3k}{(2\pi)^3} V_{\tau\tau'}(\boldsymbol{q}', \boldsymbol{k}|\boldsymbol{P}) \\ \frac{Q_{\tau\tau'}(\boldsymbol{k}, \boldsymbol{P})}{W - E_{\boldsymbol{P}+\boldsymbol{k},\tau} - E_{\boldsymbol{P}-\boldsymbol{k},\tau'}} G_{\tau\tau'}(\boldsymbol{k}, \boldsymbol{q}|\boldsymbol{P}, W). \tag{5}$$

The labels of PESs and NESs are suppressed. In this study, the Bonn potential was chosen as the realistic *NN* interaction $V_{\tau\tau'}$ [21]. $\boldsymbol{P} = \frac{1}{2}(\boldsymbol{k}_1 + \boldsymbol{k}_2)$ and $\boldsymbol{k} = \frac{1}{2}(\boldsymbol{k}_1 - \boldsymbol{k}_2)$ are the center-of-mass and the relative momenta of the two interacting nucleons with momenta $\boldsymbol{k}_1$ and $\boldsymbol{k}_2$, respectively. The initial, intermediate, and final relative momenta of the two nucleons are $\boldsymbol{q}, \boldsymbol{k}$, and $\boldsymbol{q}'$, respectively. The *NN* scattering in the nuclear medium is restricted with the Pauli operator $Q_{\tau\tau'}(\boldsymbol{k}, \boldsymbol{P})$.

Equations (1), (3), (4), and (5) constitute a coupled system that must be solved in a self-consistent manner. After the convergence of SPPs, the single-particle and bulk properties of nuclear matter can be calculated straightforwardly [29, 32, 55].

3 Results and discussion

In SNM, the Dirac masses for the nucleons calculated using the MIA and projection methods were both quantitatively close to the results obtained in the full Dirac space [48]. However, the situation changed dramatically in ANM. Figure 1 shows the isospin splitting of the Dirac mass $(M^*_{\mathrm{D,n}} - M^*_{\mathrm{D,p}})/M$ calculated using the RBHF theory as a function of the asymmetry parameter $\alpha = (\rho_{\mathrm{n}} - \rho_{\mathrm{p}})/\rho$. The projection method finds that in ANM there is $M^*_{\mathrm{D,n}} - M^*_{\mathrm{D,p}} < 0$, whereas the MIA method resulted in an opposite sign $M^*_{\mathrm{D,n}} - M^*_{\mathrm{D,p}} > 0$. The density shown in Fig. 1 is the empirical saturation density $\rho = 0.16\ \mathrm{fm}^{-3}$, and the opposite sign persisted at higher densities. This contradiction, which is well known since 1997 [46], has been clarified

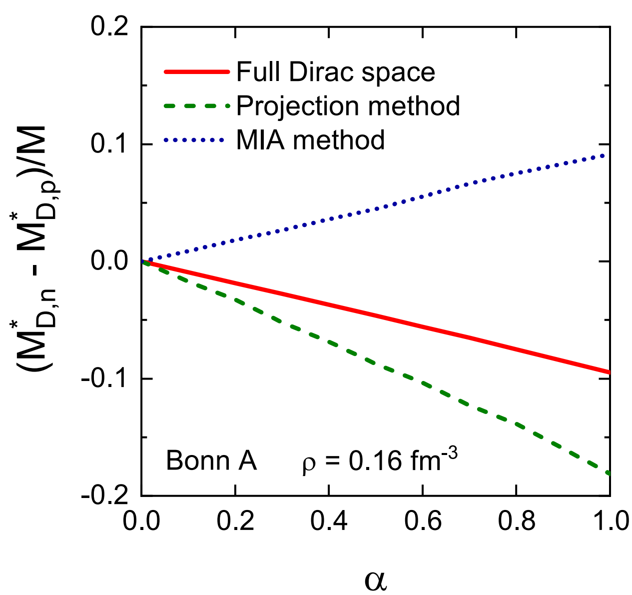

Fig. 1 (Color online) The isospin splittings of Dirac masses $(M^*_{\mathrm{D,n}} - M^*_{\mathrm{D,p}})/M$ as functions of the asymmetry parameter α obtained using the RBHF theory in the full Dirac space (red solid), the projection method (olive dashed), and the MIA method (blue dotted). The density was fixed at the normal nuclear saturation density of $\rho = 0.16\ \mathrm{fm}^{-3}$. The *NN* interaction Bonn A was used. The results for pure neutron matter with $\alpha = 1$ were obtained using linear extrapolations

recently in Ref. [48] by considering the PESs and NESs simultaneously. Comparing to the RBHF results calculated in the full Dirac space, as shown in Fig. 1, the projection method obtained a qualitatively consistent isospin dependence of the Dirac mass with overestimated amplitudes, whereas the MIA method resulted in an opposite sign.

It is still unclear why the MIA method succeeded in SNM but failed in ANM. To reach the answer, we notice that this method has two essential procedures. The first procedure is known as the *assumption procedure*, which assumes that the scalar potential and the timelike component of the vector potential are momentum independent and the spacelike component of the vector potential is negligible, that is,

$$U_{S,\tau}(p) \approx U_{S,\tau}, \quad U_{0,\tau}(p) \approx U_{0,\tau}, \quad U_{V,\tau}(p) \approx 0. \tag{6}$$

The second procedure is known as the *extraction procedure*, which extracts the two constants $U_{S,\tau}$ and $U_{0,\tau}$ from the single-particle potential energy $U_\tau(k)$ at two momenta (k_1^τ, k_2^τ).

$$U_\tau(k_1^\tau) = \frac{M + U_{S,\tau}}{\sqrt{(k_1^\tau)^2 + (M + U_{S,\tau})^2}} U_{S,\tau} + U_{0,\tau}, \tag{7a}$$

$$U_\tau(k_2^\tau) = \frac{M + U_{S,\tau}}{\sqrt{(k_2^\tau)^2 + (M + U_{S,\tau})^2}} U_{S,\tau} + U_{0,\tau}. \tag{7b}$$

The quantity $U_\tau(k)$ in Eq. (7) is calculated as $(M_\tau^*/E_{k,\tau}^*)\Sigma_\tau^{++}(k)$.

The RBHF calculations in the full Dirac space provided an opportunity to analyze in detail the isospin splitting of the Dirac mass. In the following, we try to study further by testing separately the two procedures of the MIA method from the perspective in the full Dirac space.

First, we applied the *assumption procedure* (6) in the full Dirac space, that is, the quantities $U_{S,\tau}(p)$ in Eq. (3a) and $U_{0,\tau}(p)$ in Eq. (3b) were assumed to be momentum independent and were calculated at the Fermi momentum k_F^τ, whereas $U_{V,\tau}(p)$ in Eq. (3c) was set to zero. The newly obtained quantities $U_{S,\tau}$ and $U_{0,\tau}$ were used to update the Dirac spinors and G matrix for the next iterations. When SPPs converged, we calculated the binding energies per nucleon for SNM and pure neutron matter (PNM). Figure 2 shows that the *E*/*A* values for SNM and PNM were nearly similar to those obtained using the RBHF theory in the full Dirac space. This indicates that the *assumption procedure* is reasonable for describing the bulk properties of nuclear matter.

Figure 3b shows the Dirac masses of the neutron and proton obtained in the full Dirac space using the *assumption procedure*. The density was fixed at $\rho = 0.16\ \mathrm{fm}^{-3}$. The relationship $M_{D,n}^* - M_{D,p}^* < 0$ was obtained, which was consistent with the result obtained using the RBHF theory in the full Dirac space, as shown in Fig. 3a. This indicates that the

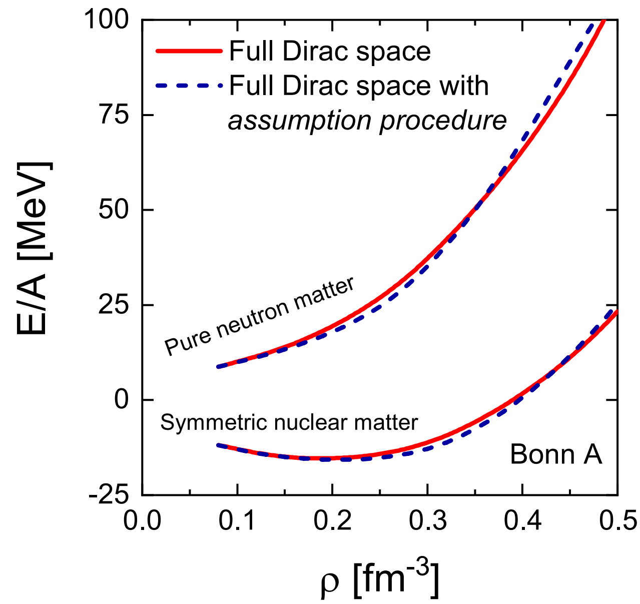

Fig. 2 (Color online) Binding energies per nucleon *E*/*A* of SNM and PNM as functions of the nucleon density ρ calculated in the full Dirac space using the *assumption procedure*. For comparison, the self-consistent results obtained using the RBHF theory in the full Dirac space are also shown

assumption procedure is not sufficient to obtain an opposite sign when the isospin splitting of the Dirac mass in ANM is calculated.

Second, we tested the influence of the *extraction procedure* (7) from the perspective in the full Dirac space. Starting from the converged $U_\tau(p)$ obtained using the RBHF theory in the full Dirac space, we extracted the two constants $U_{S,\tau}$ and $U_{0,\tau}$ using Eq. (7) with two selected momenta $(0.7k_F^\tau, k_F^\tau)$ and subsequently calculated the Dirac mass. The resulting isospin splitting of the Dirac mass is shown in Fig. 3c. It can be observed that $M_{D,n}^* - M_{D,p}^* > 0$ was obtained for the entire region of the asymmetry parameter α, which is opposite to results obtained in the full Dirac space (Fig. 3a). This indicates that the *extraction procedure* (7) resulted in the opposite sign of the isospin splitting of the Dirac mass.

To further investigate how the opposite isospin dependence of the Dirac mass resulted from the *extraction procedure*, Eq. (7) is solved to obtain a formal expression of the Dirac mass. We start from the case of SNM and suppress the isospin indexes for moment. When $M \simeq 1000$ MeV, $U_S \simeq -400$ MeV, and $k_F = 1.34\ \mathrm{fm}^{-1}$, $k_1 = 0.7k_F$ and $k_2 = k_F$ resulted in $[k_1/(M + U_S)]^2 \simeq 0.1 \ll 1$, $[k_2/(M + U_S)]^2 \simeq 0.2 \ll 1$. This allowed the square root in Eq. (7) to be expanded to first order,

$$U(k) = U_S - \frac{1}{2}\frac{U_S}{(M + U_S)^2}k^2 + U_0, \tag{8}$$

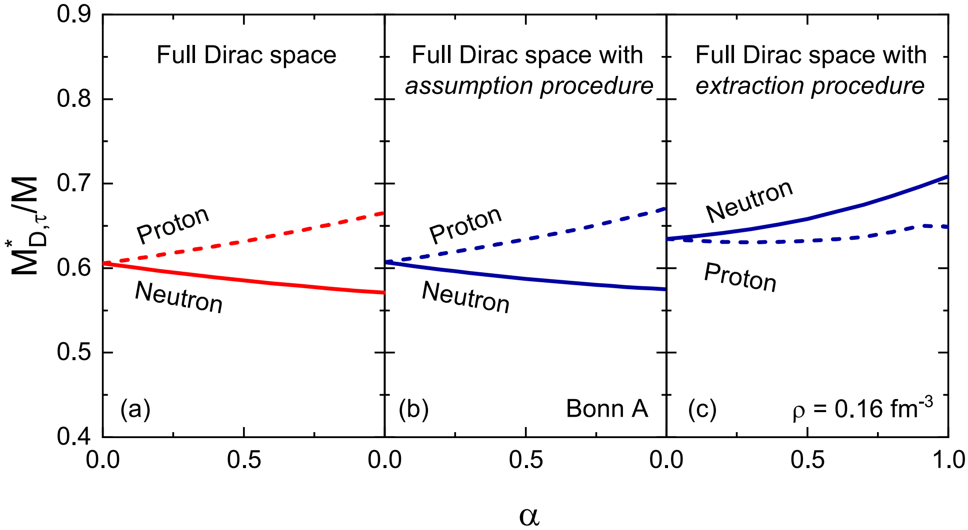

Fig. 3 (Color online) Dirac masses for neutron (solid lines) and proton (dashed lines) as functions of the asymmetric parameter α at density $\rho = 0.16\ \mathrm{fm}^{-3}$ calculated using the RBHF theory **a** in the full Dirac space, **b** using the *assumption procedure*, and **c** using the *extraction procedure*. Details can be found in the text

which indicates a quadratic form of the single-particle potential energy $U(k)$. Using Eq. (8), the difference between $U(k_2)$ and $U(k_1)$ was obtained directly, as follows:

$$U(k_2) - U(k_1) = -\frac{1}{2}\frac{U_S}{(M+U_S)^2}\left(k_2^2 - k_1^2\right). \tag{9}$$

For simplicity, we considered the limit that the two momenta k_1 and k_2 were extremely close and thus were denoted as k. In this case, Eq. (9) can be written as a quadratic equation for M_D^*/M.

$$f(k)(M_D^*/M)^2 + M_D^*/M - 1 = 0, \tag{10}$$

where the dimensionless function $f(k)$ is defined as:

$$f(k) \equiv \lim_{\substack{k_2 \to k \\ k_1 \to k}} 2M\frac{U(k_2) - U(k_1)}{k_2^2 - k_1^2} = M\frac{U'(k)}{k}. \tag{11}$$

The derivative $U'(k)$ describes the momentum dependence of the single-particle potential energy $U(k)$.

In Fig. 4a, the single-particle potential energy $U_\tau(k)$, which was obtained in the full Dirac space for SNM and ANM with $\alpha = 0.5$ and $\rho = 0.16\ \mathrm{fm}^{-3}$, is shown as a function of momentum k. It was found that $U_\tau(k)$ was a monotonic function of k. Therefore, the function $f(k)$ was positive definite, and the solution of Eq. (10) is as follows:

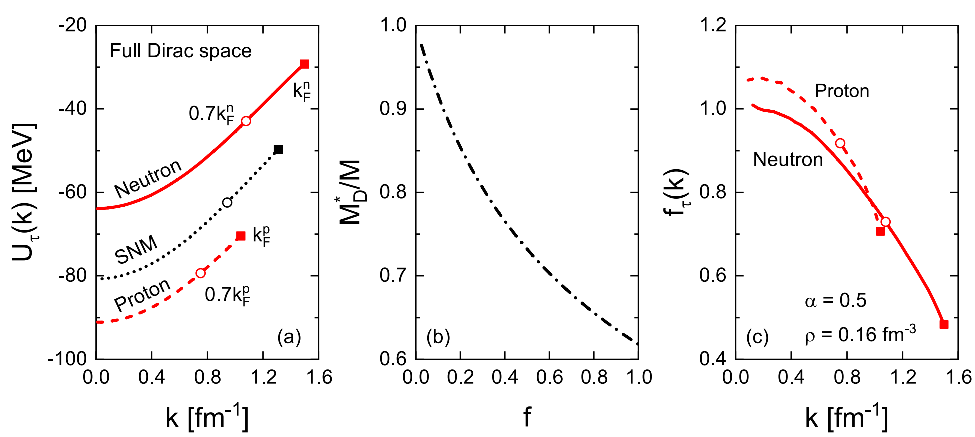

Fig. 4 (Color online) **a** Single-particle potential energy $U_\tau(k)$ obtained in the full Dirac space as a function of momentum k. The cases for SNM and ANM with $\alpha = 0.5$ and $\rho = 0.16\ \mathrm{fm}^{-3}$ are shown. The momenta $0.7k_F^\tau$ and k_F^τ are highlighted with empty dots and solid squares, respectively. **b** Dirac mass M_D^*/M as a function of dimensionless quantity f in Eq. (12). **c** Dimensionless function f (11) obtained in the full Dirac space as a function of momentum k. The notations for lines and symbols are the same as in panel (a)

$$M_{\mathrm{D}}^{*}/M = \frac{\sqrt{1+4f(k)}-1}{2f(k)}. \tag{12}$$

Figure 4(b) shows that the Dirac mass M_{D}^{*}/M decreased with increasing f. Therefore, the sign of $M_{\mathrm{D,n}}^{*} - M_{\mathrm{D,p}}^{*}$ was opposite to that of $f_{\mathrm{n}}(k_{\mathrm{n}}) - f_{\mathrm{p}}(k_{\mathrm{p}})$, that is,

$$\begin{cases} M_{\mathrm{D,n}}^{*} - M_{\mathrm{D,p}}^{*} < 0, & \text{if} \quad f_{\mathrm{n}}(k_{\mathrm{n}}) > f_{\mathrm{p}}(k_{\mathrm{p}}), \\ M_{\mathrm{D,n}}^{*} - M_{\mathrm{D,p}}^{*} > 0, & \text{if} \quad f_{\mathrm{n}}(k_{\mathrm{n}}) < f_{\mathrm{p}}(k_{\mathrm{p}}). \end{cases} \tag{13}$$

Figure 4c shows the function $f_{\tau}(k)$ for nucleon τ obtained in the full Dirac space. It was observed that $f_{\tau}(k)$ decreased with increasing k. Generally, there was $f_{\mathrm{n}}(k) < f_{\mathrm{p}}(k)$ for $k < k_{\mathrm{F}}^{\mathrm{p}}$. This indicates that the momentum dependence of $U_{\mathrm{n}}(k)$ was weaker than that of $U_{\mathrm{p}}(k)$.

In practice, one usually chooses $k_1^{\tau} = 0.7k_{\mathrm{F}}^{\tau}$ and $k_2^{\tau} = k_{\mathrm{F}}^{\tau}$ [29, 48]. For ANM with $\alpha > 0$, the Fermi momentum for neutron $k_{\mathrm{F}}^{\mathrm{n}}$ was larger than that for proton, that is, $k_{\mathrm{F}}^{\mathrm{n}} > k_{\mathrm{F}}^{\mathrm{p}}$. The symbols in panels (a) and (c) in Fig. 4 indicate that this selection resulted in $k_{\mathrm{n}} > k_{\mathrm{p}}$ and $f_{\mathrm{n}}(k_{\mathrm{n}}) < f_{\mathrm{p}}(k_{\mathrm{p}})$. Specifically, starting from the self-consistent $U_{\tau}(k)$ obtained in the full Dirac space, the choices $(0.7k_{\mathrm{F}}^{\mathrm{n}}, k_{\mathrm{F}}^{\mathrm{n}})$ for neutron and $(0.7k_{\mathrm{F}}^{\mathrm{p}}, k_{\mathrm{F}}^{\mathrm{p}})$ for proton resulted in $f_{\mathrm{n}}(k_{\mathrm{n}}) \approx 0.6$ and $f_{\mathrm{p}}(k_{\mathrm{p}}) \approx 0.8$. Based on the analysis in Eq. (13), the isospin splitting of the Dirac mass $M_{\mathrm{D,n}}^{*} - M_{\mathrm{D,p}}^{*} > 0$ emerged. This explains the reason why the MIA method resulted in an opposite isospin splitting of the Dirac mass in ANM.

In Eq. (8), the *extraction procedure* forcibly assumes that the momentum dependence of the single-particle potential energy is in a quadratic form, where the strength $-\frac{1}{2}\frac{U_{\mathrm{S}}}{(M+U_{\mathrm{S}})^2}$ is solely determined by the scalar potential U_{S}. In ANM, the momentum dependence of $U_{\mathrm{n}}(k)$ was generally weaker than that of $U_{\mathrm{p}}(k)$, as shown in Fig. 4c. This resulted in $U_{\mathrm{S,n}} > U_{\mathrm{S,p}}$ and the opposite sign of the isospin splitting of the Dirac mass $M_{\mathrm{D,n}}^{*} - M_{\mathrm{D,p}}^{*} > 0$.

Based on the aforementioned analysis of the MIA method, the RBHF theory provides a robust understanding of the isospin splitting of the Dirac mass derived from realistic *NN* interactions. This framework effectively establishes ab initio predictions for the momentum dependence of nuclear mean fields and the isovector properties of in-medium *NN* interactions. Moreover, it potentially provides constraints on the relativistic energy density functional [56], enhances our understanding of pseudospin and spin-orbit splittings observed in exotic nuclei [57–59], and promotes the study of neutron-rich systems such as neutron stars [40, 60].

4 Summary

In summary, the relativistic Brueckner–Hartree–Fock (RBHF) theory plays an important role in deriving nuclear many-body properties from realistic nucleon–nucleon interactions. In comparison with the results obtained self-consistently in the full Dirac space, the momentum-independent approximation (MIA) method leads to opposite isospin splitting of the Dirac mass in asymmetric nuclear matter (ANM). The performance of this method was explored in detail in the full Dirac space viewpoint. The *assumption procedure* of the MIA method, which assumes that single-particle potentials are momentum independent, is not a sufficient condition that directly leads to the opposite sign of the isospin splitting of the Dirac mass, whereas the *extraction procedure* of the MIA method, which extracts single-particle potentials from single-particle potential energy, is found to be responsible for the opposite isospin splitting of the Dirac mass. A formal expression of the Dirac mass was obtained by solving approximately a set of equations involved in the *extraction procedure*. With the typical choice of momenta adopted in practical MIA calculations, the opposite isospin splitting of the Dirac mass was found. We conclude that the opposite isospin splitting of the Dirac mass emerges from the fact that the *extraction procedure* forcibly assumes the momentum dependence of the single-particle potential energy to be a quadratic form where the strength is solely determined by the constant scalar potential. This study substantially improves our understanding on the isospin splitting of the Dirac mass using the RBHF theory.

Acknowledgements The authors thank the discussion with Professor Peter Ring.

Author contributions All authors contributed to the study conception and design. Material preparation, data collection, and analysis were performed by Pianpian Qin, Qiang Zhao and Sibo Wang. The first draft of the manuscript was written by Sibo Wang, and all authors commented on previous versions of the manuscript. All authors read and approved the final manuscript.

Data availability The data that support the findings of this study are openly available in Science Data Bank at https://cstr.cn/31253.11.sciencedb.j00186.00425 and https://doi.org/10.57760/sciencedb.j00186.00425.

Declarations

Conflict of interest The authors declare that they have no conflict of interest.

References

1. M. Baldo, C. Maieron, Equation of state of nuclear matter at high baryon density. J. Phys. G Nucl. Part. Phys. **34**, R243 (2007). https://doi.org/10.1088/0954-3899/34/5/R01
2. B.R. Barrett, P. Navratil, J.P. Vary, Ab initio no core shell model. Prog. Part. Nucl. Phys. **69**, 131 (2013). https://doi.org/10.1016/j.ppnp.2012.10.003
3. G. Hagen, T. Papenbrock, M. Hjorth-Jensen et al., Coupled-cluster computations of atomic nuclei. Rep. Prog. Phys. **77**, 096302 (2014). https://doi.org/10.1088/0034-4885/77/9/096302
4. J. Carlson, S. Gandolfi, F. Pederiva et al., Quantum Monte Carlo methods for nuclear physics. Rev. Mod. Phys. **87**, 1067 (2015). https://doi.org/10.1103/RevModPhys.87.1067
5. H. Hergert, S. Bogner, T. Morris et al., The in-medium similarity renormalization group: a novel ab initio method for nuclei. Phys. Rep. **621**, 165 (2016). https://doi.org/10.1016/j.physrep.2015.12.007
6. S. Shen, H. Liang, W. Long et al., Towards an ab initio covariant density functional for nuclear structure. Prog. Part. Nucl. Phys. **109**, 103713 (2019). https://doi.org/10.1016/j.ppnp.2019.103713
7. K.A. Brueckner, C.A. Levinson, H.M. Mahmoud, Two-body forces and nuclear saturation. I. Central Forces. Phys. Rev. **95**, 217 (1954). https://doi.org/10.1103/PhysRev.95.217
8. B.D. Day, Elements of the Brueckner-Goldstone theory of nuclear matter. Rev. Mod. Phys. **39**, 719 (1967). https://doi.org/10.1103/RevModPhys.39.719
9. F. Coester, S. Cohen, B. Day, Variation in nuclear-matter binding energies with phase-shift-equivalent two-body potentials. Phys. Rev. C **1**, 769 (1970). https://doi.org/10.1103/PhysRevC.1.769
10. P. Grangé, A. Lejeune, M. Martzolff et al., Consistent three-nucleon forces in the nuclear many-body problem. Phys. Rev. C **40**, 1040 (1989). https://doi.org/10.1103/PhysRevC.40.1040
11. M. Baldo, I. Bombaci, G.F. Burgio, Microscopic nuclear equation of state with three-body forces and neutron star structure. Astron. Astrophys. **328**, 274 (1997). https://doi.org/10.1063/1.1737143
12. W. Zuo, A. Lejeune, U. Lombardo et al., Interplay of three-body interactions in the EOS of nuclear matter. Nucl. Phys. A **706**, 418 (2002). https://doi.org/10.1016/S0375-9474(02)00750-9
13. X.R. Zhou, G.F. Burgio, U. Lombardo et al., Three-body forces and neutron star structure. Phys. Rev. C **69**, 018801 (2004). https://doi.org/10.1103/PhysRevC.69.018801
14. Z.H. Li, U. Lombardo, H.-J. Schulze et al., Nuclear matter saturation point and symmetry energy with modern nucleon-nucleon potentials. Phys. Rev. C **74**, 047304 (2006). https://doi.org/10.1103/PhysRevC.74.047304
15. Z.H. Li, U. Lombardo, H.-J. Schulze et al., Consistent nucleon-nucleon potentials and three-body forces. Phys. Rev. C **77**, 034316 (2008). https://doi.org/10.1103/PhysRevC.77.034316
16. M.R. Anastasio, L.S. Celenza, C.M. Shakin, Nuclear saturation as a relativistic effect. Phys. Rev. Lett. **45**, 2096 (1980). https://doi.org/10.1103/PhysRevLett.45.2096
17. M.R. Anastasio, L.S. Celenza, C.M. Shakin, Relativistic effects in the Bethe-Brueckner theory of nuclear matter. Phys. Rev. C **23**, 2273 (1981). https://doi.org/10.1103/PhysRevC.23.2273
18. R. Brockmann, R. Machleidt, Nuclear saturation in a relativistic Brueckner–Hartree–Fock approach. Phys. Lett. B **149**, 283 (1984). https://doi.org/10.1016/0370-2693(84)90407-6
19. C.J. Horowitz, B.D. Serot, The relativistic two-nucleon problem in nuclear matter. Nucl. Phys. A **464**, 613 (1987). https://doi.org/10.1016/0375-9474(87)90370-8
20. B. ter Haar, R. Malfliet, Equation of state of dense asymmetric nuclear matter. Phys. Rev. Lett. **59**, 1652 (1987). https://doi.org/10.1103/PhysRevLett.59.1652
21. R. Machleidt, The meson theory of nuclear forces and nuclear structure. Adv. Nucl. Phys. **19**, 189 (1989). https://doi.org/10.1007/978-1-4613-9907-0_2
22. F. Sammarruca, B. Chen, L. Coraggio et al., Dirac–Brueckner–Hartree–Fock versus chiral effective field theory. Phys. Rev. C **86**, 054317 (2012). https://doi.org/10.1103/PhysRevC.86.054317
23. T. Jaroszewicz, S.J. Brodsky, Z diagrams of composite objects. Phys. Rev. C **43**, 1946 (1991). https://doi.org/10.1103/PhysRevC.43.1946
24. G.E. Brown, Relativistic effects in nuclear physics. Phys. Scr. **36**, 209 (1987). https://doi.org/10.1088/0031-8949/36/2/003
25. B.D. Serot, J.D. Walecka, The relativistic nuclear many-body problem. Adv. Nucl. Phys. **16**, 1 (1986)
26. R. Brockmann, R. Machleidt, Relativistic nuclear structure. I. Nuclear Matter. Phys. Rev. C **42**, 1965 (1990). https://doi.org/10.1103/PhysRevC.42.1965
27. G.Q. Li, R. Machleidt, R. Brockmann, Properties of dense nuclear and neutron matter with relativistic nucleon-nucleon interactions. Phys. Rev. C **45**, 2782 (1992). https://doi.org/10.1103/PhysRevC.45.2782
28. D. Alonso, F. Sammarruca, Microscopic calculations in asymmetric nuclear matter. Phys. Rev. C **67**, 054301 (2003). https://doi.org/10.1103/PhysRevC.67.054301
29. H. Tong, X.-L. Ren, P. Ring et al., Relativistic Brueckner–Hartree–Fock theory in nuclear matter without the average momentum approximation. Phys. Rev. C **98**, 054302 (2018). https://doi.org/10.1103/PhysRevC.98.054302
30. C. Wang, J. Hu, Y. Zhang et al., Properties of nuclear matter in relativistic Brueckner–Hartree–Fock model with high-precision charge-dependent potentials. J. Phys. G: Nucl. Part. Phys. **47**, 105108 (2020). https://doi.org/10.1088/1361-6471/aba423
31. T. Gross-Boelting, C. Fuchs, A. Faessler, Covariant representations of the relativistic Brueckner T-matrix and the nuclear matter problem. Nucl. Phys. A **648**, 105 (1999). https://doi.org/10.1016/S0375-9474(99)00022-6
32. E.N.E. van Dalen, C. Fuchs, A. Faessler, The relativistic Dirac–Brueckner approach to asymmetric nuclear matter. Nucl. Phys. A **744**, 227 (2004). https://doi.org/10.1016/j.nuclphysa.2004.08.019
33. E.N.E. van Dalen, C. Fuchs, A. Faessler, Effective nucleon masses in symmetric and asymmetric nuclear matter. Phys. Rev. Lett. **95**, 022302 (2005). https://doi.org/10.1103/PhysRevLett.95.022302
34. E.N.E. van Dalen, C. Fuchs, A. Faessler, Momentum, density, and isospin dependence of symmetric and asymmetric nuclear matter properties. Phys. Rev. C **72**, 065803 (2005). https://doi.org/10.1103/PhysRevC.72.065803
35. E.N.E. van Dalen, C. Fuchs, A. Faessler, Dirac–Brueckner–Hartree–Fock calculations for isospin asymmetric nuclear matter based on improved approximation schemes. Eur. Phys. J. A **31**, 29 (2007). https://doi.org/10.1140/epja/i2006-10165-x
36. C. Nuppenau, Y. Lee, A. MacKellar, Ambiguities in the Dirac–Brueckner approach. Nucl. Phys. A **504**, 839 (1989). https://doi.org/10.1016/0375-9474(89)90011-0
37. S. Wang, Q. Zhao, P. Ring et al., Nuclear matter in relativistic Brueckner–Hartree–Fock theory with Bonn potential in the full Dirac space. Phys. Rev. C **103**, 054319 (2021). https://doi.org/10.1103/PhysRevC.103.054319
38. W.-H. Long, N.V. Giai, J. Meng, Density-dependent relativistic Hartree–Fock approach. Phys. Lett. B **640**, 150 (2006). https://doi.org/10.1016/j.physletb.2006.07.064
39. L.-W. Chen, C.M. Ko, B.-A. Li, Isospin-dependent properties of asymmetric nuclear matter in relativistic mean field models. Phys. Rev. C **76**, 054316 (2007). https://doi.org/10.1103/PhysRevC.76.054316

40. B.-A. Li, B.-J. Cai, L.-W. Chen et al., Nucleon effective masses in neutron-rich matter. Prog. Part. Nucl. Phys. **99**, 29 (2018). https://doi.org/10.1016/j.ppnp.2018.01.001
41. R. An, S. Sun, L.-G. Cao et al., Constraining nuclear symmetry energy with the charge radii of mirror-pair nuclei. Nucl. Sci. Tech. **34**, 119 (2023). https://doi.org/10.1007/s41365-023-01269-1
42. S.-N. Wei, Z.-Q. Feng, Properties of collective flow and pion production in intermediate-energy heavy-ion collisions with a relativistic quantum molecular dynamics model. Nucl. Sci. Tech. **35**, 15 (2024). https://doi.org/10.1007/s41365-024-01380-x
43. M. Jaminon, C. Mahaux, Effective masses in relativistic approaches to the nucleon-nucleus mean field. Phys. Rev. C **40**, 354 (1989). https://doi.org/10.1103/PhysRevC.40.354
44. F.-Y. Wang, J.-P. Yang, X. Chen et al., Probing nucleon effective mass splitting with light particle emission. Nucl. Sci. Tech. **34**, 94 (2023). https://doi.org/10.1007/s41365-023-01241-z
45. N. Van Giai, B.V. Carlson, Z. Ma et al., Dirac–Brueckner–Hartree–Fock approach: from infinite matter to effective lagrangians for finite systems. J. Phys. G **37**, 064043 (2010). https://doi.org/10.1088/0954-3899/37/6/064043
46. S. Ulrych, H. Müther, Relativistic structure of the nucleon self-energy in asymmetric nuclei. Phys. Rev. C **56**, 1788 (1997). https://doi.org/10.1103/PhysRevC.56.1788
47. S. Wang, H. Tong, C. Wang, Nuclear matter within the continuous choice in the full Dirac space. Phys. Rev. C **105**, 054309 (2022). https://doi.org/10.1103/PhysRevC.105.054309
48. S. Wang, H. Tong, Q. Zhao et al., Asymmetric nuclear matter and neutron star properties in relativistic ab initio theory in the full Dirac space. Phys. Rev. C **106**, L021305 (2022). https://doi.org/10.1103/PhysRevC.106.L021305
49. S. Wang, H. Tong, Q. Zhao et al., Neutron-proton effective mass splitting in neutron-rich matter. Phys. Rev. C **108**, L031303 (2023). https://doi.org/10.1103/PhysRevC.108.L031303
50. H. Tong, J. Gao, C. Wang et al., Properties of ^{208}Pb predicted from the relativistic equation of state in the full Dirac space. Phys. Rev. C **107**, 034302 (2023). https://doi.org/10.1103/PhysRevC.107.034302
51. S. Wang, H. Tong, C. Wang et al., Tensor-force effects on nuclear matter in relativistic ab initio theory. Sci. Bull. **69**, 2166 (2024). https://doi.org/10.1016/j.scib.2024.05.013
52. H. Tong, C. Wang, S. Wang, Nuclear matter and neutron stars from relativistic Brueckner–Hartree–Fock theory. Astrophys. J. **930**, 137 (2022). https://doi.org/10.3847/1538-4357/ac65fc
53. S. Wang, C. Wang, H. Tong, Exploring universal characteristics of neutron star matter with relativistic ab initio equations of state. Phys. Rev. C **106**, 045804 (2022). https://doi.org/10.1103/PhysRevC.106.045804
54. X. Qu, H. Tong, C. Wang et al., Neutron matter properties from relativistic Brueckner–Hartree–Fock theory in the full Dirac space. Sci. China-Phys. Mech. Astron. **66**, 242011 (2023). https://doi.org/10.1007/s11433-022-2048-3
55. T. Katayama, K. Saito, Properties of dense, asymmetric nuclear matter in Dirac–Brueckner–Hartree–Fock approach. Phys. Rev. C **88**, 035805 (2013). https://doi.org/10.1103/PhysRevC.88.035805
56. Q. Zhao, Z. Ren, P. Zhao et al., Covariant density functional theory with localized exchange terms. Phys. Rev. C **106**, 034315 (2022). https://doi.org/10.1103/PhysRevC.106.034315
57. H. Liang, J. Meng, S.-G. Zhou, Hidden pseudospin and spin symmetries and their origins in atomic nuclei. Phys. Rep. **570**, 1 (2015). https://doi.org/10.1016/j.physrep.2014.12.005
58. X.-N. Cao, X.-X. Zhou, M. Fu et al., Research on the influence of quadrupole deformation and continuum effects on the exotic properties of ^{15,17,19}B with the complex momentum representation method. Nucl. Sci. Tech. **34**, 25 (2023). https://doi.org/10.1007/s41365-023-01177-4
59. E.-B. Huo, K.-R. Li, X.-Y. Qu et al., Continuum Skyrme Hartree–Fock–Bogoliubov theory with Green's function method for neutron-rich Ca, Ni, Zr, and Sn isotopes. Nucl. Sci. Tech. **34**, 105 (2023). https://doi.org/10.1007/s41365-023-01261-9
60. B.Y. Sun, W.H. Long, J. Meng et al., Neutron star properties in density-dependent relativistic Hartree–Fock theory. Phys. Rev. C **78**, 065805 (2008). https://doi.org/10.1103/PhysRevC.78.065805